Biophysical Chemistry 41 (1991) 131–141
Elsevier Science Publishers B.V., Amsterdam

BIOCHE 01584

Computer simulation of surface-induced aggregation of ferritin

Manne Stenberg * and Håkan Nygren

Department of Histology, University of Göteborg, P.O.Box 33031 S-400 33 Göteborg (Sweden)

(Received 10 february 1991; accepted 6 March 1991)

Abstract

Models are presented describing the transient mass-transport limited adsorption and cluster growth of ferritin at a solid surface. Computer simulations are carried out on a hexagonal lattice using a computer model that can be characterized as a two-dimensional stochastic cellular automaton allowing different rules regarding association, lateral interaction and dissociation to be incorporated in the model. The fractal dimensions of individual clusters were extracted from simulated aggregates and for similar rules found to be consistent with literature values on reversible diffusion-limited aggregation in two dimensions. The distribution of clusters versus free surface were shown to be affected by neighbor-dependent association probability. Low fractal dimension clusters were generated by a combination of strong lateral cohesion and neighbor-dependent dissociation to the bulk. By comparing computer simulated aggregation to experimental electron micrographs of adsorbed ferritin layers it is suggested that neighbor-dependent association, neighbor-dependent dissociation and lateral interactions are important factors in the complex dynamics of adsorbed protein layers.

Keywords: Protein adsorption; Two-dimensional aggregation; Computer simulation; Cellular automata; Ferritin

1. Introduction

If a solid surface is introduced into a stable protein solution it is immediately covered by adsorbed protein molecules. During the adsorption process the surface actually induces aggregation of protein molecules and these aggregates show fractal properties [1–3]. This finding has initiated computer simulations to model the initial diffusion-limited aggregation (DLA-clustering) [4]. It was found that the adsorbed protein molecules must most probably be mobile along the surface with a diffusion constant considerably lower ($5 \cdot 10^{-4}$) than in the bulk solution. The initial aggregation could be well described by reversible DLA-clustering (at $\theta = 0.015$) but at higher surface coverage of proteins the presented model could not account for the low experimentally observed fractal dimension. At a surface coverage $\theta = 0.1$ large clusters with fractal dimension $d_f = 0.98 \pm 0.15$ have been seen [2]. Typical clusters of this kind are shown in Fig. 1. The simulations presented in the present study aimed at finding some possible mechanisms responsible for the low fractal dimensions measured on aggregates of adsorbed protein molecules.

* To whom correspondence should be addressed.

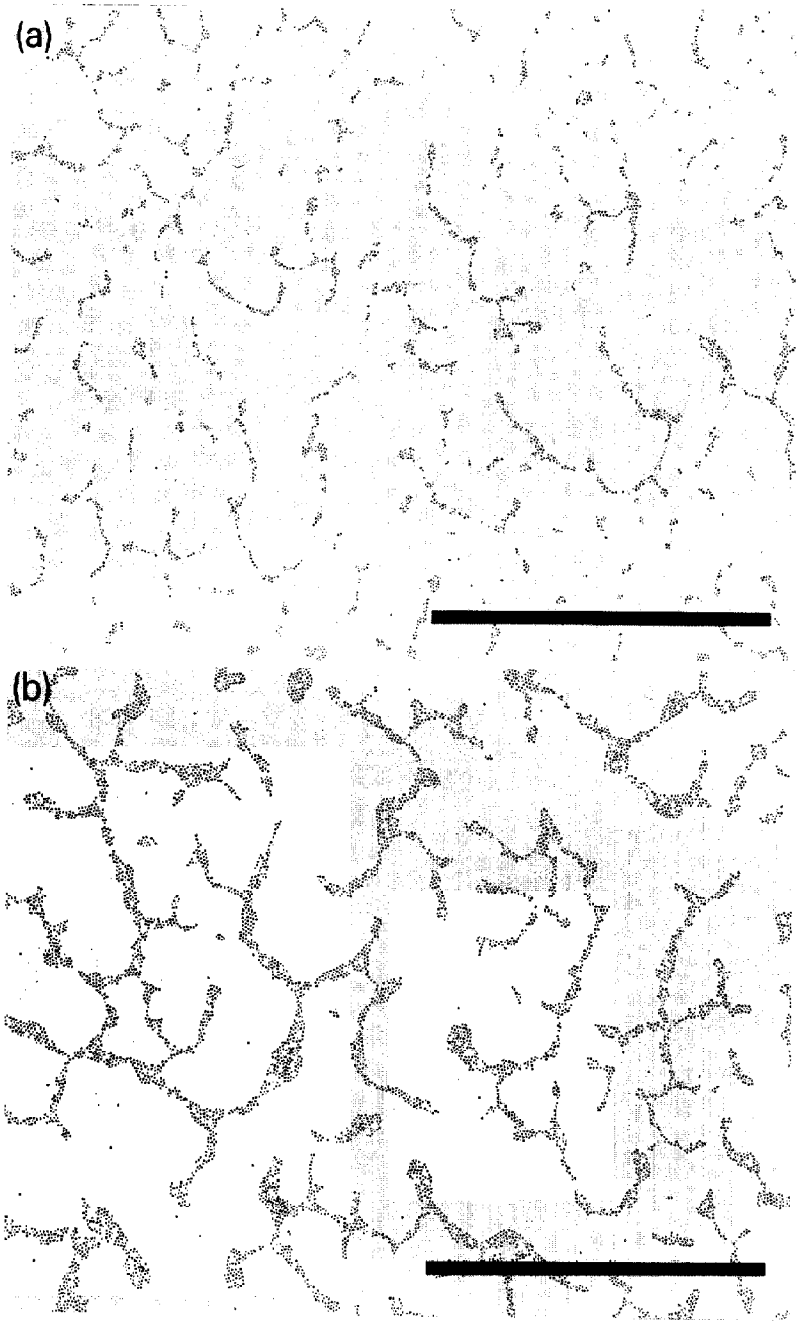

Fig. 1. Electron micrograph of adsorbed ferritin molecules on a hydrophobic silicon-dioxide surface. The dark spots are the electron-dense iron cores in the protein molecules. The surface has been incubated in a PBS buffer solution containing 10 μg/ml ferritin and the amount bound is diffusion limited (from ref. 3) (Bar is 1 μm). (a) Incubation time 100 s and surface coverage $\theta = 0.06$, (b) Incubation time 280 s and surface coverage $\theta = 0.1$.

When dealing with systems where nearest-neighbor interactions are considered and where particles may suddenly appear at different sites at the surface it is natural to use computer models known as cellular automata [5]. Our simulation methods are close to that of two-dimensional cel-

lular stochastic automata which have been used for studying two-dimensional phase transitions [6].

2. Simulation methods

2.1 Association

The simulations were carried out for an experimental situation where a surface is introduced at time zero into a solution containing the adsorbing molecules at a homogeneous initial concentration. By assuming that adsorbed molecules do not leave the surface we get the diffusion limited adsorbed amount as

$$n_s = \frac{1}{\sqrt{\pi}} n_0 \sqrt{D_b t} \tag{1}$$

where n_s is the surface concentration in number per unit area at time t, D_b is the diffusion constant in the bulk solution and n_0 is the bulk concentration in number per unit volume. For a hexagonal lattice the maximum surface concentration in terms of number per unit area is

$$n_{sm} = \frac{1}{2\sqrt{3}\, r_0^2} \tag{2}$$

where r_0 is the particle radius. The initial volume fraction ϕ_0 is

$$\phi_0 = n_0 \tfrac{4}{3}\pi r_0^3 \tag{3}$$

and thus, for a hexagonal lattice the diffusion limited surface coverage can be written

$$\theta = \frac{n_s}{n_{sm}} = \left(\frac{3}{\pi}\right)^{3/2} \phi_0 \frac{\sqrt{D_b t}}{r_0} \tag{4}$$

Each position in the hexagonal lattice is updated in discrete time steps equal to the mean time needed for moving one lattice position by surface diffusion. In two dimensions the mean displacement Δr after a time Δt is

$$\Delta r = 2\sqrt{D_s \Delta t} \tag{5}$$

where D_s is the surface diffusion constant. With $\Delta r = 2r_0$ we get the time increment as

$$\Delta t = r_0^2 / D_s \tag{6}$$

After T iterations we get $t = T \cdot \Delta t$ and by combining eqs. (4) and (t) we get the normalized relation

$$\theta(T) = C\sqrt{T} \tag{7}$$

where the parameter C is related to initial concentration and the respective diffusion constants by

$$C = \left(\frac{3}{\pi}\right)^{3/2} \phi_0 \sqrt{\frac{D_b}{D_s}} \tag{8}$$

In the simulations we choose to specify C by giving the total number of iterations T_t and the corresponding final coverage θ_t so that

$$C = \theta_t / \sqrt{T_t} \tag{9}$$

We can use eq. (7) to calculate the number of new particles at iteration $T+1$ and every iteration is started by increasing the coverage by an amount calculated from the relation:

$$\Delta\theta = \theta_t \sqrt{\frac{(T+1)}{T_t}} - \theta(T) \tag{10}$$

When adding new particles a site is chosed at random and analysed with respect to the number of nearest neighbors, n. The association or sticking probability p_a is depending on the number of nearest neighbors, n, at the specific site. Repeated trials are performed until a successful association is achieved. Two different association algorithms were tested. In the first algorithm, A1, the sticking probability $p_a = 1$ regardless of the number of nearest neighbor. In the second association algorithm, A2, the sticking probability $p_a = 1$ only for sites with $n > 0$ and $p_a = p_{a1} \ll 1$ for sites with no nearest neighbor. In the second algorithm A2, we used a value $p_{a1} = 2^{-9}$.

After adjustment of the total number of particles every lattice-position is analysed with respect to its neighbor. From the neighbor situation it will be decided whether the particle will dissociate or make a lateral jump.

2.2 Dissociation

Bulk diffusion is assumed to be much faster than surface diffusion in the present model which

also includes the diffusion limited boundary condition of zero concentration close to the surface. Therefore, all particles that dissociate are assumed to reassociate immediately. A dissociation probability p_d is calculated for each particle based on the number of nearest neighbor, n. Three different dissociation algorithms were tested:

D1: $p_d(n) = 0$ for all n

D2: $p_d(n) = p_{d1}$ for all n

D3: $p_d(n) = p_{d1}$ for $n < 4$

$p_d(4) > p_d(3)$

$p_d(5) > p_d(4)$

$p_d(6) > p_d(5)$

In the first algorithm D1, there is no dissociation. In the second dissociation algorithm D2, particles dissociate at a constant rate independent of the number of nearest neighbor. In the third algorithm D3, dissociation probability is very low and constant when there are few nearest neighbors. When the number of nearest neighbors exceeds 3 instability in the adsorbed film begin to show up which will give increased dissociation probability. Values used for the dissociation probabilities in the four models are shown in Table 1.

After dissociation the particles are forced to reassociate immediately to keep the number of particles determined by the diffusion from bulk.

Table 1

Value of the dissociation probability p_d for different numbers of nearest neighbors, n, and the different dissociation models tested. In model D2 a constant dissociation probability is used. In model D3 dissociation becomes more probable for high numbers of nearest neighbors

n	D1	D2	D3
0	0	2^{-15}	2^{-21}
1	0	2^{-15}	2^{-21}
2	0	2^{-15}	2^{-21}
3	0	2^{-15}	2^{-21}
4	0	2^{-15}	2^{-18}
5	0	2^{-15}	2^{-15}
6	0	2^{-15}	2^{-12}

Reassociation are carried out as described before with one of two different association algorithms.

2.3. Lateral jumps

For particles which have not dissociated a direction of jumping is chosen at random and the probability of jumping is determined from the neighbor distribution. In this work we have three types of neighbors, defined by the direction of jumping as shown in Fig. 2. Jumping with an A-type nearest neighbor requires the creation of extra particle–liquid interface whereas jumping with a B-type nearest neighbor can be done by sliding along this neighbor. Jumping with a C-type next-nearest neighbor gives a reduction of particle–liquid interface and the probability of jumping may increase in this situation if there is an attractive potential acting over some distance.

In the prescence of at least one nearest neighbor the probability of jumping p_J is reduced:

$$p_J(n_A, n_B) = f_A^{n_A} f_B^{n_B} f_C^{n_C} p_0$$

where p_0 denotes the intrinsic probability of jumping for aggregated particles, f_A the reduction due to an A-type neighbor, f_B the reduction due to a B-type neighbor, f_C the increase due to a C-type neighbor, n_A the number of A-type neighbors, n_B the number of B-type neighbors, and n_C the number of C-type neighbors. By the factor f_C we may introduce an attractive force acting some distance between particles.

Three different lateral jump algorithms (Fig. 3) were tested:

L1: $f_A = f_B = f_C = 1$, $p_0 < 1$.

L2: $f_A < 1$, $f_B = f_C = 1$, $p_0 = 1$.

L3: $f_A < 1$, $f_B = 1$, $f_C > 1$, $p_0 = 1$, $p_J(n_A, n_B) \leq 1$.

In the first algorithm, L1, the binding strength is independent of the number of neighbors whereas in the second algorithm, L2, binding strength increases with number of nearest neighbors of type A. In the third algorithm L3 also the next-nearest

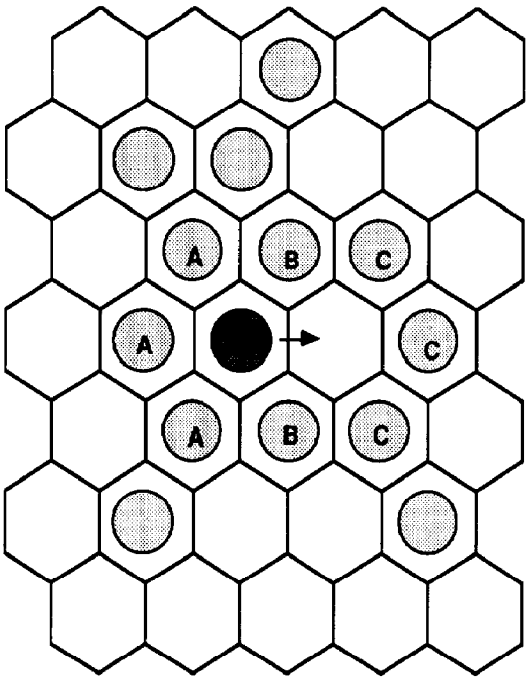

Fig. 2. Simulations are carried out on a hexagonal lattice. The fate of every lattice position is up-dated in discrete time steps. For every occupied lattice site a direction of jumping is chosen at random and this direction defines A- and B-type nearest neighbors and C-type next-nearest neighbors as shown in the figure. Provided there is an empty site in the jumping direction the probability of jumping is determined by rules based on the number of A-, B- and C-type neighbors.

neighbors of type C may influence the jumping probability. The prescence of C-type next-nearest neighbors increases the probability of jumping up

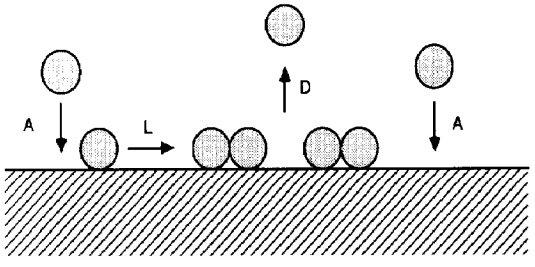

Fig. 3. Different rules regarding association (A), dissociation (D) and lateral diffusion (L) are used in the simulations. A dissociated particle reassociates immediately at some other lattice position, keeping the number of particles unchanged at the surface. Dissociation as well as association probability may be determined by the number of neighbors giving different association and dissociation algorithms.

to the limit $p_J = 1$. Values used for the jump probabilities in the three models are:

L1: $f_A = f_B = f_C = 1,\ p_0 = 2^{-9}$

L2: $f_A = 2^{-3},\ f_B = 1,\ f_C = 1,\ p_0 = 2^{-6}$

L3: $f_A = 2^{-3},\ f_B = 1,\ f_C = 2^2,\ p_0 = 2^{-6}$

The simulations were carried out on a 256×256 hexagonal lattice with periodic boundary conditions. The resulting aggregates were analysed by measuring the radius of gyration R_g for an s cluster defined as

$$R_g = \left(\sum_{i=1}^{s} r_i^2 / s \right)^{1/2} \tag{11}$$

where r_i is the distance of a site from the center of mass. Average values of R_g were then plotted against s and fitted to the form

$$R_g = \text{const} \cdot s^{\rho} \tag{12}$$

where for scale-invariant clusters the exponent ρ should be related to the fractal dimension d_f by $d_f = 1/\rho$. The mean and standard deviation of the fractal dimension were evaluated from three different simulations in each case.

3. Results

In Fig. 4 we see the result of growing reversible DLA-clusters without dissociation into the bulk. In Fig. 4a the lateral dissociation is independent on the number of neighbors. No characteristic patterns can be seen in this case. In Fig. 4b both lateral dissociation and lateral association is dependent on the number of neighbors by lateral jump algorithm L3. This algorithm corresponds to increased cohesion forces in the aggregates and we can see how the particles tend to condense into circular discs. Analysis of the radius of gyration (Fig. 8) shows that the distributions of radius of gyration can be described by eq. (12). For the first simulation in Fig. 4a we find a fractal dimension $d_f = 1.51 \pm 0.07$ in agreement with earlier literature values of two-dimensional reversible DLA-clusters: $d_f = 1.54 \pm 0.08$ [7] and $d_f = 1.57 \pm 0.06$

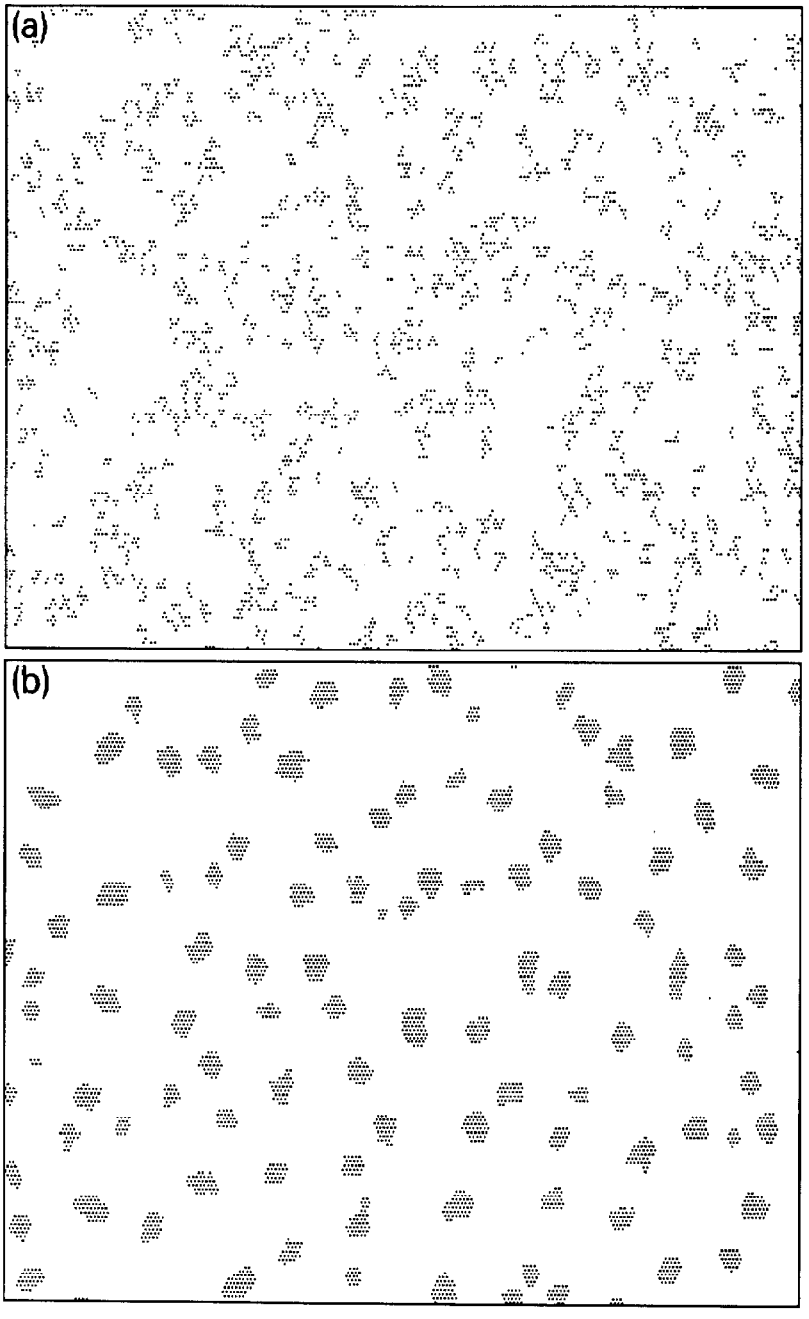

Fig. 4. Reversible DLA-clusters with no dissociation into the bulk and an association rule A1, where the sticking coefficient $p_a = 1$ for all sites. The clusters shown are generated after 10^5 iterations at a coverage $\theta = 0.1$ ($C = 3.16 \cdot 10^{-4}$). The different rules for lateral jumps are (see text for definition of parameters): (a) Lateral jump algorithm L1: $f_A = f_B = f_C = 1$, $p_0 = 2^{-9}$; (b) lateral jump algorithm L3: $f_A = 2^{-3}$, $f_B = 1$, $f_C = 2^2$, $p_0 = 2^{-6}$.

[8]. However, for the condensed aggregates in Fig. 4b we get a higher fractal dimension $d_f = 1.91 \pm 0.03$ which is close to the Euclidean dimension two showing the the aggregates have almost lost their fractal properties.

One characteristic of experimental clusters is

that larger areas without particles will develope and that the particles tend to grow in clusters of clusters (Fig. 1). In Fig. 5 is shown that this is what happens if the association algorithm is changed so that the sticking probability is reduced for all sites without neighbors. With no other changes in the simulation rules there will be a slight increase in the fractal dimension (Table 2).

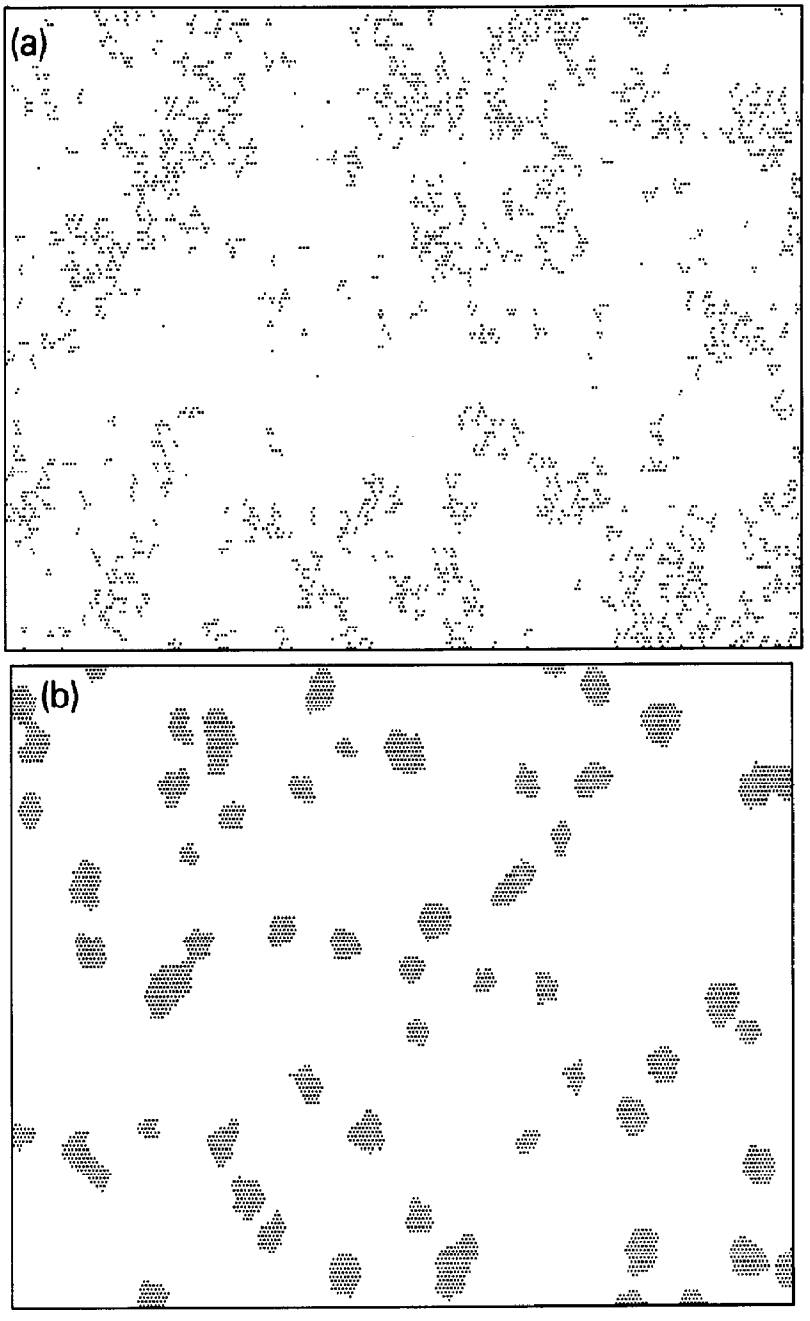

Fig. 5. Reversible DLA-clusters as in Fig. 4 but with a different association rule A2, with a reduced sticking probability $p_a = 2^{-9}$ for sites without neighbors. (a) Lateral jump algorithm L1, and (b) Lateral jump algorithm L3.

Table 2

Fractal dimension d_f for transient reversible DLA-clusters generated after 10^5 iterations to a final coverage $\theta = 0.1$. The table shows the influence of different association algorithms A1 and A2, dissociation algorithms D1, D2 and D3 and lateral jump algorithms L1, L2 and L3

	A1D1	A2D1	A2D2	A1D3	A2D3
L1	1.51 ± 0.07	1.67 ± 0.06	1.54 ± 0.04	1.56 ± 0.07	1.59 ± 0.05
L2	1.84 ± 0.04	1.30 − 2.0	1.40 − 1.80	1.37 ± 0.05	1.48 ± 0.02
L3	1.91 ± 0.03	1.25 − 2.0	1.25 − 2.0	0.9 − 1.7	1.22 ± 0.04

In Fig. 5b it can be seen that in this simulation some clusters tend to coalesce and form some big more linear aggregates. This will result in a slight deviation from eq. (12) when radius of gyration versus aggregate size is analysed as shown in Fig. 9a.

Introducing dissociation as a possible mechanism will in some cases have a dramatic effect on the shape of the aggregates. In Fig. 6 we can see that the change is rather small for the first lateral algorithm L1 but very great for the third algorithm L3. In Fig. 6b we can see the effect of introducing the dissociation algorithm D3 where dissociation is more probable for particles with many neighbors. The clusters formed are still rather dense at small distances but there is a strong tendency to form prolonged linear aggregates. For these aggregates no well defined fractal dimension can be estimated. Instead the corresponding fractal dimension varies between 0.9 and 1.7.

By combining the effect of varying association probabilities and neighbor dependent dissociation we arrive at the simulations presented in Fig. 7. The difference is still not so big for the first lateral jump algorithm L1 but with the third lateral jump algorithm L3 we now see quite long linear aggregates forming in accordance with the experimental patterns shown in Fig. 1. However, compared to the simulations the experimental patterns show more threadlike structures. From the plot in Fig. 9 it can be seen that in this case the radius of gyration follows eq. (12) for at least one decade. The fractal dimension was estimated to $d_f = 1.22 \pm 0.04$ which is not far from the measurements on the experimental clusters of Fig. 1.

Table 2 summarizes the estimated fractal dimensions obtained with different combinations of the presented algorithms. It is seen that for the lateral jump algorithm L1 all values are close to the earlier reported values of reversible DLA-clusters. With the lateral jump algorithm L2 the lowest fractal dimension found was around 1.3. For some intermediate combinations of the different algorithms the log–log plot of R_g versus s (Fig. 8) was not linear and in these cases the slope range are given in Table 2.

4. Discussion

In this study we present some models of diffusion limited cluster growth at an interface which could produce the characteristic patterns found experimentally [3]. Diffusion limited adsorbtion from bulk solution is combined with different rules for reorganization in the adsorbed layer. We have shown that many different aggregation patterns may be obtained. The basic idea is that aggregation together with instability and dissociation from dense regions in the protein film could be responsible for the observed low-dimension clusters. Clusters with low fractal dimensions can be grown by combining strong cohesion in the growing clusters with dissociation from dense cluster regions. From Table 2 we can see how the introduction of phase-separation and dissociation may change the fractal dimension of the clusters and we can cover the range $d_f = 1.2$–2. Low dimension clusters in two dimensions have earlier been reported for diffusion limited aggregation of silica microspheres where it was found a fractal dimension $d_f = 1.2 \pm 0.15$ [9]. A model of clustering of polarizable clusters has been presented to account for these low fractal dimensions [10]. Two-dimensional simulations of this model gener-

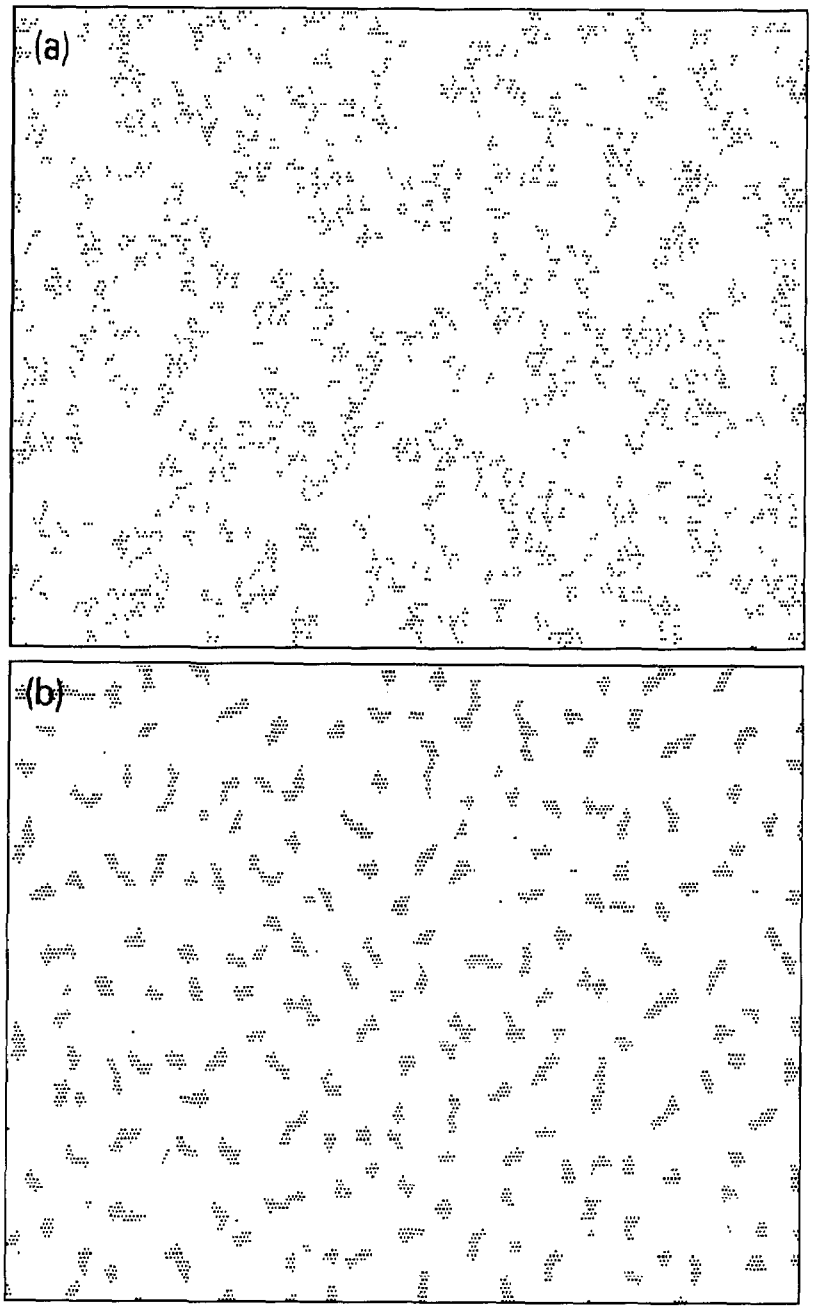

Fig. 6. Reversible DLA-clusters as in Fig. 4 with association rule A1, but with dissociation of particles into the bulk. Dissociation rule D3 has been used, see Table 1. (a) Lateral jump algorithm L1, and (b) Lateral jump algorithm L3.

ated clusters with $d_f = 1.26 \pm 0.06$. However, the close hexagonal dense packing at short distances in the ferritin aggregates makes this model less attractive.

The simulations are restricted to the simplified situation where the amount bound is limited by diffusion from the solution and also to different diffusion-limited aggregation models where the

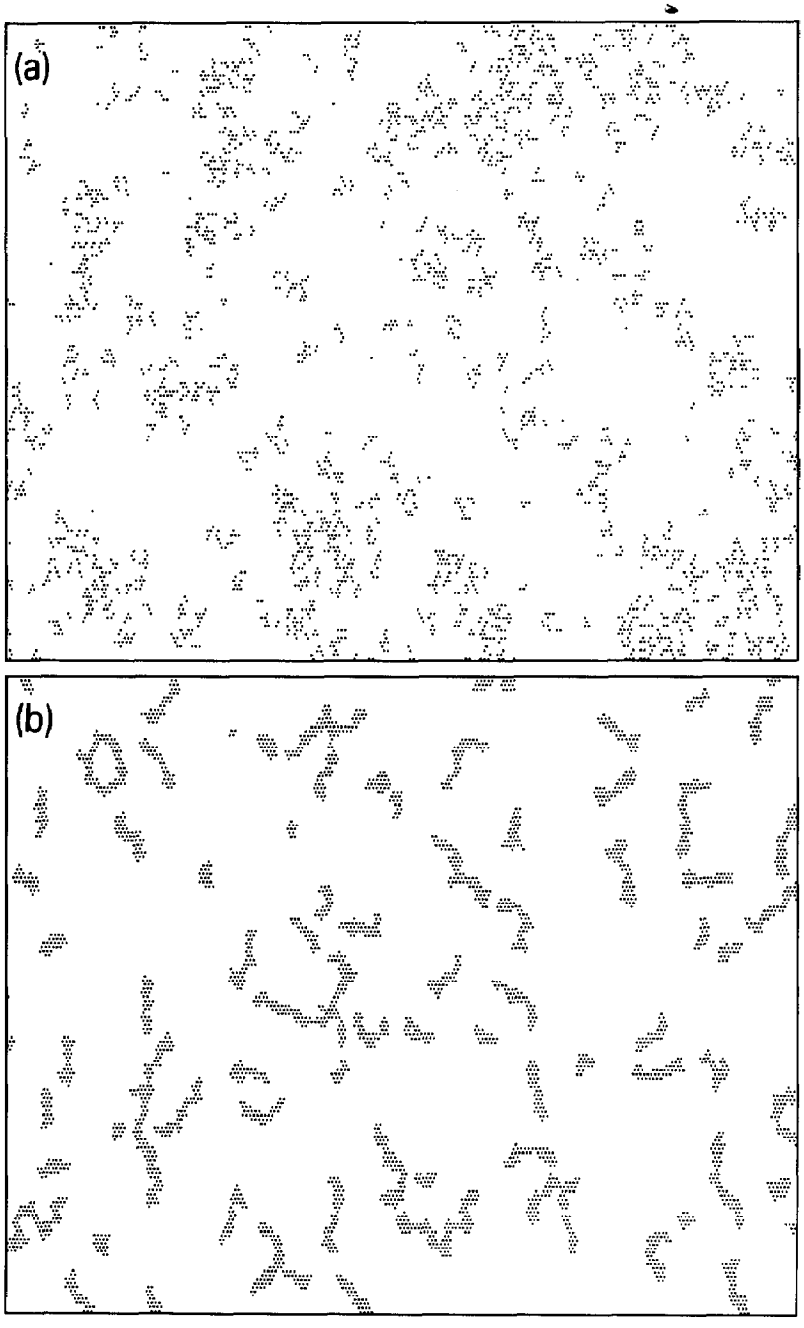

Fig. 7. Reversible DLA-clusters as in Fig. 4 but with a different association rule A2 and with dissociation of particles into the bulk. Dissociation rule D3 has been used, see Table 1. (a) Lateral jump algorithm L1. (b) Lateral jump algorithm L3.

sticking coefficient is one for colliding particles. Another restriction has been to study rules valid only for homogeneous interaction between protein molecules. If the aggregation of the protein molecules is instead governed by interaction between specific sites on the protein surfaces more complex rules must be considered. The tendency of the experimental aggregates to form threadlike struc-

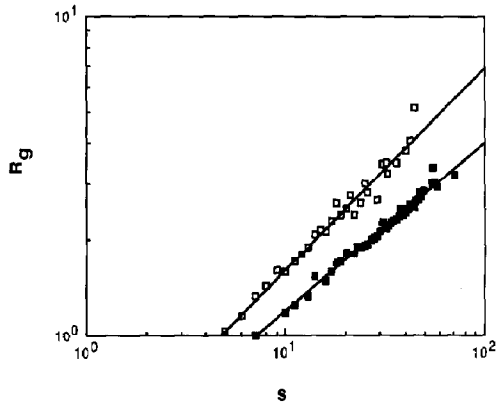

Fig. 8. A log–log plot of the radius of gyration R_g versus cluster mass s for reversible DLA-clusters ($C = 3.16 \cdot 10^{-4}$, $\theta = 0.1$): (□) A1D1L1 Fig. 4a (slope $\rho = 0.635$), and (■) A1D1L3, Fig. 4b (slope $\rho = 0.528$).

tures with molecules in a row may be an indication to the presence of preferred sites. However, it is important to notice that a combination of lateral phase-separation and dissociation to bulk can also be the mechanism behind the formation of low fractal dimension aggregates as shown in the present study.

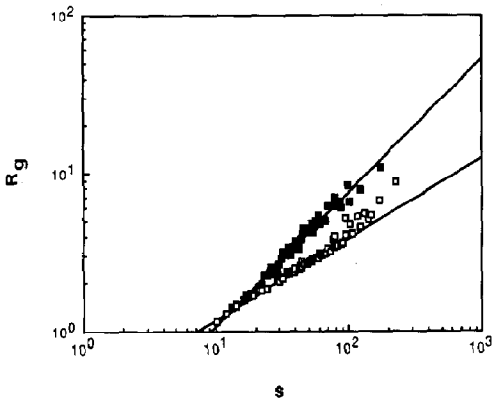

Fig. 9. A log–log plot of the radius of gyration R_g versus cluster mass s for reversible DLA-clusters ($C = 3.16 \cdot 10^{-4}$, $\theta = 0.1$): (□) A2D1L3, Fig. 5b (slope $\rho = 0.514$), and (■) A2D3L3, Fig. 7b (slope $\rho = 0.844$).

5. Conclusions

In this study we have shown that experimental patterns of surface-induced protein aggregation can not be obtained by simple growth mechanisms. Lateral interactions giving rise to phase-separation in the adsorbed layer must be combined with more complex rules. One possible mechanism for generating the experimentally observed low-dimensional fractal aggregates is to combine strong cohesion in the growing clusters with dissociation from dense cluster regions.

Acknowledgement

The present study was supported by a grant from the National Swedish Board for Technical Development (grant no. 89-468 P) and from the Swedish Medical Research Council (grant no. 12 X 06235).

References

1 H. Nygren and M. Stenberg, Prog. Colloid Polym. Sci. 82 (1990) 15.
2 H. Nygren and M. Stenberg, Biophys. Chem. 38 (1990) 67.
3 H. Nygren and M. Stenberg, Biophys. Chem. 38 (1990) 77.
4 M. Stenberg and H. Nygren, Prog. Colloid Polym. Sci. 82 (1990) 10.
5 S. Wolfram, Nature 311 (1984) 419.
6 W. Kinzel, Z. Phys. B 58 (1985) 229.
7 R. Botet and R. Jullien, Phys. Rev. Lett. 55 (1985) 1943.
8 M. Kolb, J. Phys. A Math. Gen. 19 (1986) L263.
9 A. Hurd and D. Schaefer, Phys. Rev. Lett. 54 (1985) 1043.
10 R. Jullien, Phys. Rev. Lett. 55 (1985) 1697.